High-Q Tunable Microwave Cavity Resonators and Filters using SOI-based RF MEMS Tuners

Xiaoguang Liu, *Student Member, IEEE,* Linda P. B. Katehi, *Fellow, IEEE,* William J. Chappell, *Member, IEEE* and Dimitrios Peroulis, *Member, IEEE*

***Abstract*—This paper presents the modeling, design, fabrication and measurement of MEMS-enabled continuously tunable evanescent-mode electromagnetic cavity resonators and filters with very high unloaded quality factors (Q_u). Integrated electrostatically-actuated thin diaphragms are used for the first time for tuning the frequency of the resonators/filters. An example tunable resonator with 2.6:1 ($5.0-1.9$ GHz) tuning ratio, Q_u of $300-650$ is presented. A continuously tunable 2-pole filter from 3.04 GHz to 4.71 GHz with 0.7% bandwidth and insertion loss of $3.55-2.38$ dB is also shown as a technology demonstrator. Mechanical stability measurements show that the tunable resonators/filters exhibit very low frequency drift (less than 0.5% for 3 hours) under constant bias voltage. This paper significantly expands upon previously reported tunable resonators [1].**

***Index Terms*—Evanescent-mode cavity, MEMS, quality factor, tuning, tunable filter, tunable resonator, electrostatic actuation**

I. Introduction

TUNABLE RF/Microwave filters are essential components for the next generation reconfigurable radio front-ends in wireless communication systems with multi-band and multi-standard characteristics [2]. Several technologies exist for making tunable RF/Microwave filters. Yttrium-Iron-Garnet (YIG) resonator based tunable filters are the most widely used and exhibit a very wide tuning range over multiple octaves and a very high unloaded quality factor Q_u ($10,000$ at 10 GHz) [3]. Nevertheless, the large volume (approximately 1 in^3) and high power consumption ($0.75-3$ W) of YIG based tunable filters hinder their integration into mobile communication systems. Alternative approaches have been proposed to make miniaturized tunable RF/Microwave filters. These approaches are based on micromechanical resonators [4]–[6], cavity filters [7], [8], planar transmission line resonators loaded with solid-state varactors [9], ferroelectric-tuned varactors [10]–[12] and MEMS varactors/switches [13]–[15]. These technologies have achieved either a) very high Q_u at the cost of limited tuning range (<2%), such as micro-mechanical filters [6]; or b) high tuning range at the cost of low Q_u (<200 @ 5 GHz), such as MEMS varactor tuned filters.

Recently, however, there has been some success in realizing widely tunable filters with simultaneous high-Q_u and low insertion loss using evanescent-mode cavity resonators with MEMS tuners [1], [16]–[18]. In [16], Hou et al. presented preliminary results on tunable micromachined evanescent-mode resonator with Q_u of 200 at 2.5 GHz and 120 at 4 GHz. Joshi et al. demonstrated substrate integrated evanescent-mode tunable filters with high tuning range ($2.3-4$ GHz) and high Q_u ($360-700$) [17]. Both designs use an external piezoelectric actuator as the tuning element. The well-known hysteresis and creep of piezoelectric actuators present significant system level problems for these tunable resonators and filters (see Section III for detailed discussion). In [18], Park et al. demonstrated a 2-pole evanescent-mode filter using MEMS varactor networks. The achieved tuning range and Q_u was limited to $4.3-5.5$ GHz and $273-511$ respectively. In [1], the authors of this paper demonstrated a tunable resonator with Q_u of $460-530$ in the $3.4-6.2$ GHz range. An electrostatic thin diaphragm MEMS tuner was used for its high precision, high reliability and near zero hysteresis.

In this paper, we build on our previous work and investigate the use of electrostatically-actuated evanescent-mode cavity resonators for making tunable RF/Microwave filters with simultaneous wide tuning range and high Q_u. Specifically, in relation to [1], we present the optimized results of tunable resonators with state-of-the-art performance in terms of tuning range ($1.9-5.0$ GHz, i.e. 2.6:1 ratio), Q_u ($300-650$) and stability. The modeling methodology and design trade-offs of electrostatically-actuated MEMS tuner are discussed in detail with focus on the interdependences of tuning range, actuation voltage, tuning speed and long term stability. The design, fabrication and characterization of a $3.04-4.71$ GHz two-pole tunable bandpass filter with insertion loss of $3.55-2.38$ dB is presented as a demonstrator for this technology.

The organization of this paper is as follows. In Section II, the fundamental concepts and design methods of evanescent-mode cavity resonators are reviewed and presented. Section III discusses the various design considerations and trade-offs for the electrostatic thin diaphragm MEMS tuner. Section IV presents the fabrication and assembly techniques for making the proposed tunable resonators/filters. Measurement and discussions of the fabricated tunable resonator are presented in Section V. In Section VI, the design and measurements of a 2-pole tunable bandpass filter are presented.

X. Liu, W. J. Chappell and D. Peroulis are with the School of Electrical and Computer Engineering, Purdue University, West Lafayette, IN, 47906 USA e-mail: liu79@purdue.edu, chappell@purdue.edu and dperouli@purdue.edu.

L. P. B. Katehi is with the University of California, Davis, CA, USA. email: katehi@ucdavis.edu.

This work has been supported by the Defense Advanced Research Projects Agency under the ASP Program with a subcontract from BAE Systems. The views, opinions, and/or findings contained in this article/presentation are those of the author/presenter and should not be interpreted as representing the official views or policies, either expressed or implied, of the Defense Advanced Research Projects Agency or the Department of Defense.

The authors are grateful to Hjalti H. Sigmarsson and Himanshu Joshi of Purdue University for helpful discussions and technical assistance.

II. Design of the Evanescent-mode Electromagnetic Cavity Resonator

Evanescent-mode waveguide filters have recently attracted great interest for realizing low-loss, highly-selective tunable filters for reconfigurable RF front-ends [23], [24]. Compared to half-wave cavity resonators, evanescent-mode resonators offer significant advantages. These including substantially smaller volume and weight, larger spurious-free region and improved feasibility for monolithic integration, while maintaining very high Q_u [23], [24].

The resonant characteristics of capacitive-post-loaded evanescent-mode cavity resonators are well-studied in the literature [24], [25]. The resonant frequency and Q_u are found to be functions of the cavity size, post size and the gap between the post top and cavity ceiling. In the highly-loaded case, i.e. when the capacitive gap g between the post and the cavity top wall is very small, the resonant frequency is very sensitive to g. A gap change in the order of micrometers can result in a frequency change of several GHz.

Fig. 1 shows the simulated resonant frequency and Q_u of a highly-loaded evanescent-mode cavity with a varying capacitive gap. This simulation is conducted with Ansoft HFSS, which is a Finite Element Method (FEM) based full wave electromagnetic solver [26]. The radius b and height h of the cylindrical cavity are 8 mm and 4.5 mm respectively. The post radius a is 1 mm and g is swept between $5-50$ μm. Copper (conductivity of 5.8×10^7 S/m) is used as the internal boundary of the cavity resonator. It can be seen that Q_u is in the $700-2000$ range in between $2-6$ GHz, which is much higher than lumped element and planar transmission line based resonators [27].

It is worth noting that in the highly-loaded case, the resonant wavelength is much larger than the size of the post. For example, in the above simulation, the resonant wavelength at $g=5$ μm is 133 mm whereas the radius of the post is 1 mm. Fig. 2(a) shows an approximate illustration of the electric and magnetic field inside a highly-loaded evanescent-mode cavity resonator. The uniform electric field between the cavity top and the post suggests that the region above the post can be

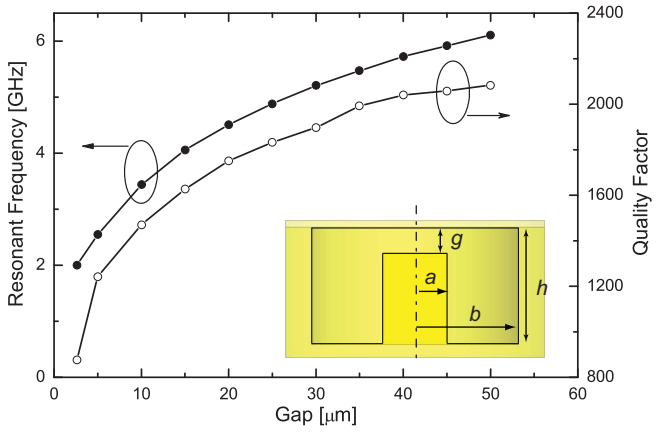

Fig. 1. Simulated resonant frequency and unloaded quality factor Q_u of an evanescent-mode resonant cavity. Dimensions of the cavity are $a=1$ mm , $b=8$ mm, $h=4.5$ mm.

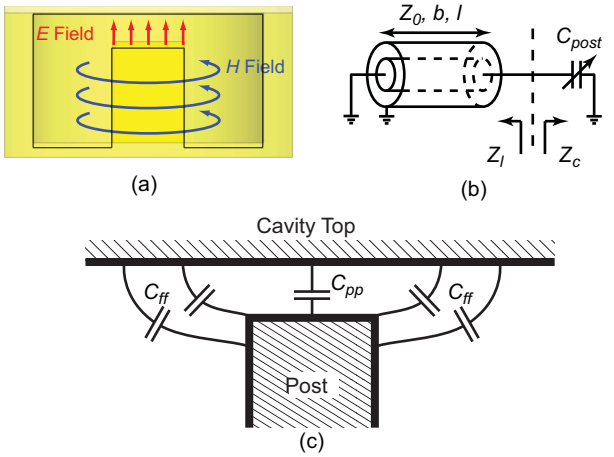

Fig. 2. Quasistatic modeling of highly-loaded evanescent-mode cavity resonator. (a) Field distribution in highly-loaded evanescent-mode resonator; (b) Equivalent circuit model; (c) Post capacitance.

modeled by a lumped capacitor, while the toroidal magnetic field around the post suggests that the post and sidewall of the cavity can be modeled by a shorted coaxial line, which represents an effective inductor at the fundamental resonant frequency.

Therefore, the resonant frequency of an evanescent-mode cavity resonator can be found by equating Z_l and Z_c, which are the impedances looking into the capacitive region and the inductive region respectively (Fig. 2(b)).

$$Z_l + Z_c = 0. \tag{1}$$

$$jZ_0 \tan\beta l + \frac{1}{j2\pi f C_{post}} = 0. \tag{2}$$

$$Z_0 \tan(2\pi f_r \frac{l}{c_0}) = \frac{1}{2\pi f_r C_{post}}, \tag{3}$$

where f_r is the resonant frequency, l is the post height, c_0 is the free space speed of light, C_{post} is the effective capacitance of the post and Z_0 is the characteristic impedance of the coaxial line, which is determined by the post diameter a and cavity diameter b.

Eqn. (3) can be solved numerically once the post capacitance C_{post} is known. Previously, C_{post} has been evaluated by using the parallel-plate capacitance C_{pp} as a first-order approximation [1], [16]. More careful modeling requires the effect of fringing field capacitance C_{ff} to be taken into consideration.

An evanescent-mode tunable cavity resonator is designed for $2-6$ GHz range as a vehicle to demonstrate the proposed concepts. To achieve size reduction and better integration with other circuit components, the evanescent-mode resonant cavity is integrated into a *Rogers TMM®-3* microwave substrate [28]. Fig. 3 shows the concept drawing of the designed resonant cavity. Copper plated vias are used to connect the top and bottom metal layer to form the evanescent-mode cavity. The capacitive post is machined from the substrate and electroplated with copper. Shorted coplanar waveguides (CPW) are used as the input and output feeding structures. The

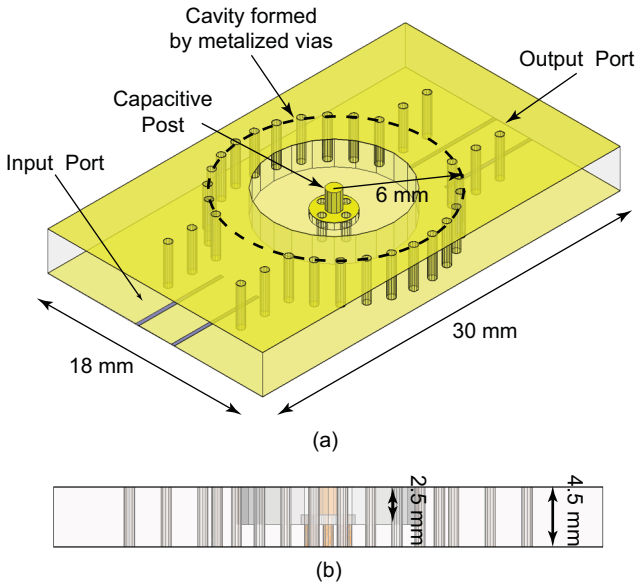

Fig. 3. Concept drawing of the evanescent-mode cavity in *Rogers TMM®-3* substrate. The MEMS actuator, which is not shown in this drawing, is to be discussed in Section III.

transverse magnetic field of the shorted CPW is coupled with the toroidal magnetic field (Fig. 2(a)) around the capacitive post to achieve input and output coupling. Dimensions of the cavity design are labeled in Fig. 3.

Fig. 4 shows the simulated resonant frequency and Q_u of the designed tunable resonator. The thickness of the top wall of the cavity (not shown in Fig. 3) is assumed to be 0.5 μm in the simulation. It can be seen that the resonant frequency changes from 2 GHz to 6 GHz when g_0 changes from 2 μm to 17 μm. This leads to a simulated Q_u change from 350 to 1100. It is obvious that a deflection of ~ 15 μm is needed to achieve a tuning ratio of $3:1$, and ~ 10 μm is needed for $2:1$. Such large deflections present challenges to the design of the MEMS tuner, which will be discussed in detail in the next section.

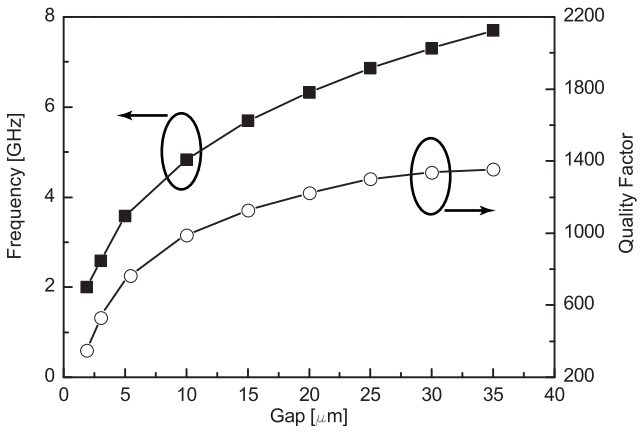

Fig. 4. Simulated resonant frequency and Q_u of designed tunable evanescent-mode cavity resonator. The MEMS actuator is assumed to have a maximum stroke of $15-20$ μm. Dimensions of the design in this simulation are shown in Fig. 3.

III. Design and Integration of MEMS Diaphragm Tuner

A. Actuation Scheme

Frequency tuning is achieved by deflecting a thin metallic diaphragm which is placed on top of the evanescent-mode cavity (Fig. 6). Several methods can be used for the actuation of the diaphragm, including electrothermal, piezoelectric and electrostatic actuations. The high power consumption and low speed of electrothermal actuation makes it undesirable for portable applications. Piezoelectric actuation consumes little power and can generate high actuation force. Joshi et al. demonstrated piezo-actuated evanescent-mode tunable filters with high Q_u and a wide tuning range [17]. However, it is well known that piezoelectric actuators have hysteresis and creep problems [19]–[22]. As an example, a piezo-actuator used in [17] is taken for deflection measurement using an Olympus LEXT® microscope. The LEXT® is a laser confocal microscope and has a measurement uncertainty of < 0.1 μm. Fig. 5 shows the deflection of the piezo-actuator with bias voltage cycled between -210 V to 210 V. Hysteresis is observed over several cycles. With the hysteresis and creep behaviors of the piezo-actuator, repeatable and reliable frequency tuning with high precision can become a system level problem.

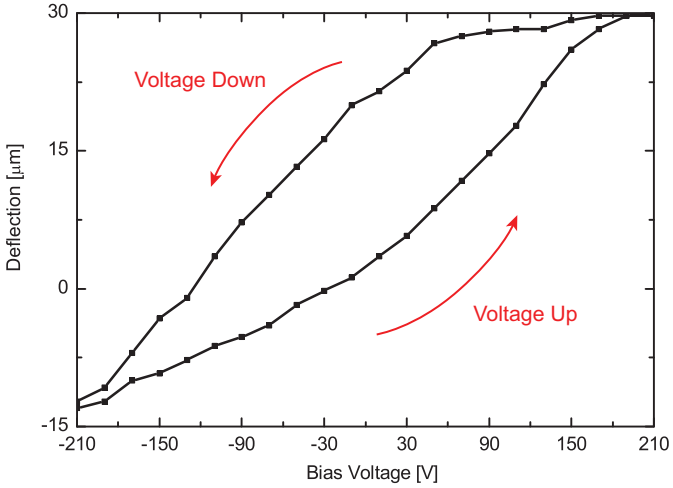

Fig. 5. Deflection measurement on a piezo-actuator used in [17] shows substantial hysteresis.

Electrostatic actuation, on the other hand, can be precise, reliable and hysteresis-free. Therefore we choose to use electrostatic actuation in this work. Fig. 6 shows a concept drawing of the electrostatic diaphragm actuator. The diaphragm consists of a layer of gold deposited on the released device layer of an silicon-on-insulator (SOI) wafer. Due to its stress-free and defect-free nature, the single-crystal silicon device layer serves as a flexible yet robust mechanical support to the gold layer. The Au-Si composite diaphragm is packaged on top of the capacitive post to form the tunable resonator. When a bias voltage is applied to the actuation electrode placed a distance d_0 above the diaphragm, electrostatic force will pull the diaphragm away from the capacitive post to change the resonant frequency. An important advantage of using a planar diaphragm is that it does not distort the natural current flow

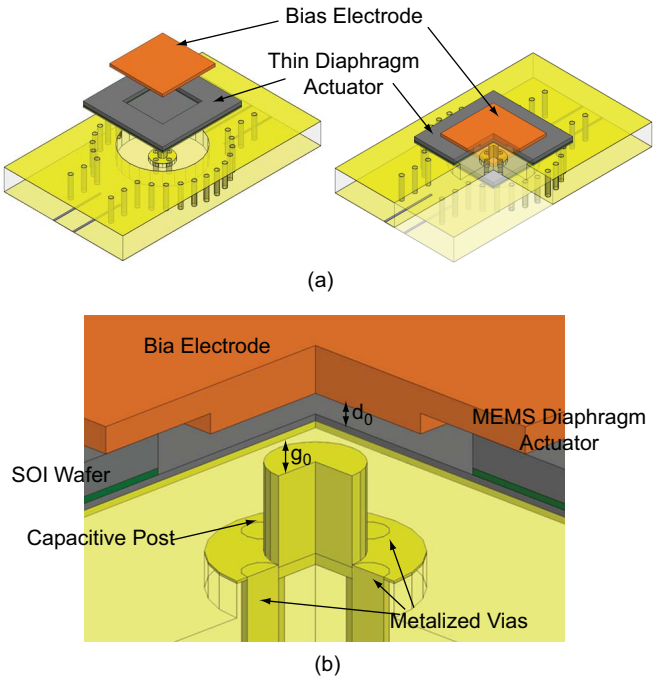

Fig. 6. Concept drawing of the MEMS thin diaphragm tuner. (a) The integration of thin diaphragm tuner with the evanescent-mode resonant cavity; (b) A close-up view of the MEMS tuner.

and preserves the high Q_u of the cavity resonator, leading to very low filter insertion loss. This design is also inherently reliable and tolerant to material and process variations due to the use of SOI-based fabrication process.

B. Electro-mechanical Considerations

Several parameters are of concern in the design of the electrostatic actuator, including tuning range, actuation voltage, tuning speed and long term stability.

1) Tuning Range

The maximum deflection of the diaphragm directly relates to the tuning ratio of the resonator. Indeed, the tuning ratio is roughly given by (4) [1]

$$R_{max} \approx \sqrt{\frac{g_0 + d_0/3}{g_0}}. \tag{4}$$

It can be seen that the tuning ratio can be increased by decreasing the initial gap g_0. However, excessively small g_0 can cause significant difficulty in the accuracy and yield of the tunable resonator. Q_u is also compromised with a small g_0. In this design, an initial gap $g_0 = 2$ μm is used with consideration given for both high tuning range and high Q_u. In order to achieve a tuning ratio of $>$ 2:1, a minimum d_0 of 30 μm is required.

2) Actuation Voltage

It is generally desirable to keep the actuation voltage as low as possible. In tunable filters with multiple resonators, the resonant frequency of each resonator must be precisely aligned according to the specific design. Therefore analog tuning of the resonant frequency is highly desirable. In the analog tuning region of an electrostatic actuator, the maximum actuation voltage can not exceed the pull-in voltage. The pull-in voltage V_{pi} of the diaphragm tuner is given by (5), in which W is the side length of the square bias electrode, d_0 is the initial actuation gap and k is the spring constant for the diaphragm [27].

$$V_{pi} = \sqrt{\frac{8kd_0^3}{27\epsilon W^2}} \tag{5}$$

The spring constant of a circular diaphragm is given by

$$k = k' + k'' = \frac{Et^3}{0.0138\ w^2} + \frac{\pi^2 \sigma t}{7.2} \tag{6}$$

where w and t are the diaphragm side length and thickness, E is the Young's modulus, and σ is the residual stress [29], [30]. As previously noted, the single crystal silicon device layer is a nearly stress free material and the residual stress is mainly due to the thin Au layer. For thin diaphragms, the k'' term dominates the spring constant value in the presence of practical residual stress ($>$ 5 MPa). For example, for a 3.5 μm thick diaphragm (0.5 μm Au on top of 3 μm single crystal silicon) with a size of 2×2 mm^2, Au residual stress of 30 MPa and a d_0 of 40 μm, the pull-in voltage is 415 V.

To lower the actuation voltage to an acceptable range, it is desirable to lower the spring constant k by reducing either the residual stress or the thickness of the Au film. However, the reduction of residual stress in the Au film is limited by fabrication process tolerances and extremely low stress ($<$ 5 MPa) is very difficult to achieve [27]. Reduction of the Au film thickness also comes with a penalty in higher RF loss. The Au skin depth at $2-6$ GHz range is $1.76-1.02$ μm. It is desirable to have a Au layer thickness larger than the skin depth at this frequency range. Careful compromise must be made in choosing Au film thickness from the mechanical point of view. Fig. 7 shows HFSS simulations of the Q_u of an evanescent-mode resonator with different Au thickness on the top wall. It can be seen that there is a significant drop in Q_u for Au thickness less than 0.5 μm at $2-6$ GHz.

Whereas a high spring constant k is limited by process tolerance and quality factor requirements, the size of the diaphragm can be increased to reduce the actuation voltage. Although a larger diaphragm has relatively insignificant impact on k (diaphragm size only comes into play in the k' term, which is dominated by the k'' term), it can accommodate a larger bias electrode, therefore reducing the required actuation voltage.

3) Long Term Mechanical Stability

Long term mechanical stability is an additional benefit of using a larger diaphragm. The high Q_u of the evanescent-mode tunable resonator makes it a promising candidate for use in very narrow band tunable filters. For such filters, frequency precision and stability is a critical

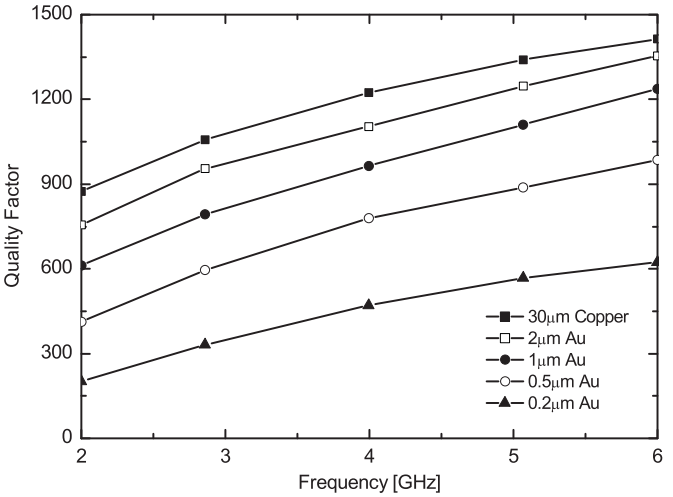

Fig. 7. Simulated Q_u with different Au thin film thickness. Cavity dimensions are the same as in Fig. 4

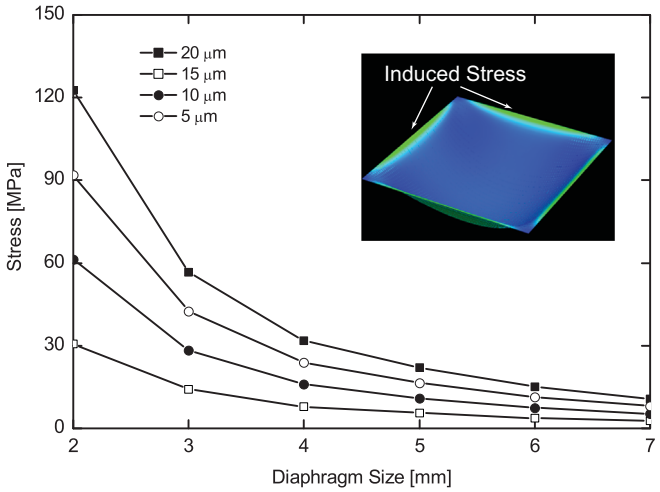

Fig. 8. Simulated induced stress in actuated square diaphragms of different sizes (side length).

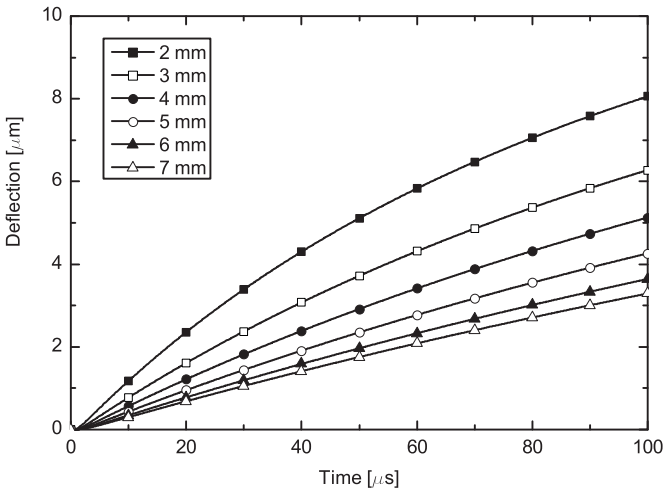

Fig. 9. Calculated actuation speed of diaphragms of varying sizes.

concern. In order to improve the frequency stability and compensate for any frequency misalignment due to fabrication tolerances, a closed-loop control system is needed to continuously monitor and adjust the bias voltage to maintain a stable frequency response. In order to ease the control loop design, the proposed tunable resonator needs to have a stable frequency response.

It is well known that material creep and viscoelasticity are important factors affecting the long term performances of MEMS devices. Creep is defined as the strain response of a material under constant stress. Viscoelasticity is referred to as the time dependent response to an applied force. It has been shown that creep/viscoelasticity leads to material property change under non-zero loading over time. These parameter changes are often characterized as an effective Young's modulus drift [31], [32].

In our tunable resonator design, the effective Young's modulus drift will result in resonant frequency shift over time. It has been shown that the effective Young's modulus drift rate is directly related to the induced stress/strain in the actuating structure. Lower stress/strain results in lower drift. Fig. 8 shows the simulated induced stresses in square diaphragms of different sizes at varying deflections. Simulation is done with the Coventorware MEMS simulation package [34]. It is shown that larger diaphragms have inherently lower stress for a given deflection. Apart from lower actuation voltage, larger diaphragms also demonstrate lower frequency drift rates.

4) Tuning Speed

The compromise of employing a relatively large diaphragm lies in slower response time due to its larger mass and smaller spring constant. For example, Fig. 9 shows the calculated actuation time for square diaphragms of varying side lengths using a simple 1-D spring-mass model [27]. The thicknesses of the Si and Au film are assumed to be 3 μm and 0.5 μm respectively. A residual stress of 30 MPa is used in the calculation and a mechanical Q of 0.1 is assumed. It can be seen from Fig. 9 that larger diaphragms take longer time to actuate. To improve the tuning speed, air vent holes can be added to the diaphragm. In such a case, the air holes may adversely affect the Q_u of the resonator.

5) Temperature Stability

Temperature stability may be another concern for the SOI-based diaphragm tuners. The use of different materials with different coefficients of thermal expansion (CTE) in the fabrication process need to be considered as well. As mentioned in Section III-B-3), however, a close-loop feedback control system can be used to compensate for any frequency drift due to environmental perturbations. This is in general necessary for high-Q tunable systems [35].

From the above discussion, it is clear that careful consideration and suitable compromises among the resonator's actuation voltage, frequency tunability, quality factor, mechanical robustness/stability, resistance to creep and tuning speed need

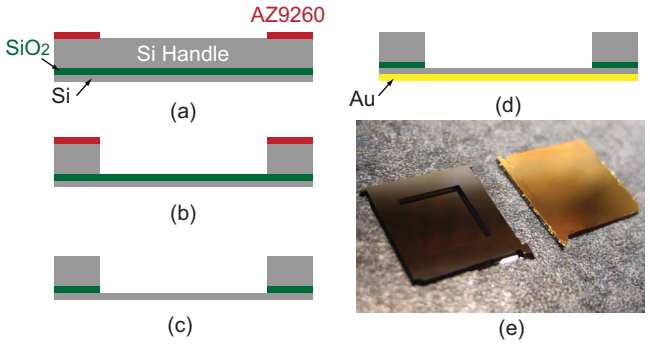

Fig. 10. Fabrication process for MEMS diaphragm: (a) AZ9260 patterning; (b) DRIE; (c) Oxide etch; (d) Au sputter; (e) Fabricated MEMS Diaphragm piece.

to be made to satisfy the requirements of a given application.

IV. Fabrication Technology

The fabrication process of the tunable resonator involves standard microfabrication processes and conventional machining techniques. It consists of three parts: 1) the SOI diaphragm piece, 2) the bias electrode piece, and 3) the cavity piece. Fig. 10-13 summarizes the fabrication process.

A. MEMS Diaphragm

The fabrication of the MEMS diaphragm starts with patterning an AZ9260 photoresist layer on the handle layer side as an etching mask for deep reactive ion etching (DRIE). The buried oxide layer has very high selectivity (> 200:1) to silicon in the DRIE process and serves as an etch stop layer. The oxide layer is etched in Buffered-Oxide Etchant (BOE) after the handle layer is etched by DRIE. The device silicon layer is released after the removal of the oxide layer. The released diaphragm is flat due to the extremely low residual stress in the device silicon layer. A 0.5 μm thick Au layer is then deposited on top of the released silicon diaphragm by DC sputtering. The sputtering condition is carefully controlled to achieve a low tensile stress in the metal layer. Fig. 11 shows an SEM image of the fabricated MEMS thin diaphragm (with the diaphragm cleaved along the anchor to reveal the cross-sectional structure.)

B. Bias Electrode

The bias electrode consists of two pieces of silicon bonded together. The thickness of the smaller piece h is controlled by timed wet etching in a 25% TMAH solution at $80°$C. The etching condition ensures < 0.1 μm thickness control and a very smooth surface finish. The two pieces are then metalized with Au on both sides and bonded together by Au-Au thermal-compression bonding at $350°$C and 50 MPa pressure. A layer of 2 μm Parylene-C is deposited on the smaller piece side to create an insulation layer for biasing.

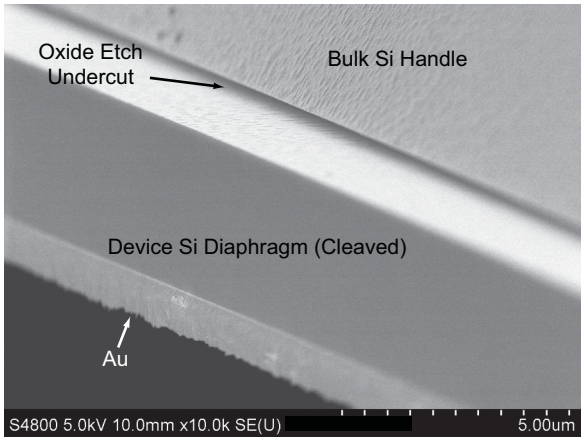

Fig. 11. SEM image of the fabricated MEMS diaphragm piece. The diaphragm is cleaved along the anchor to reveal the cross-section structures.

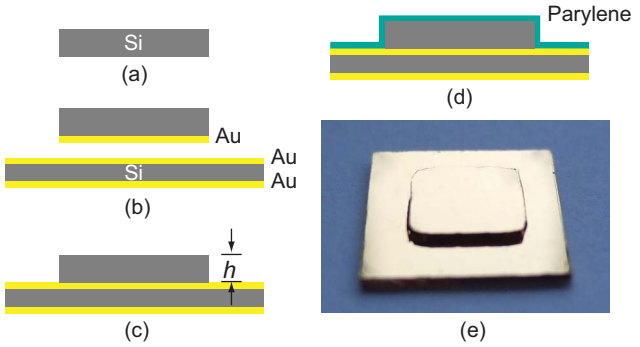

Fig. 12. Fabrication process for bias electrodes: (a) Top silicon piece; (b) Au sputter; (c) Au-Au thermal compression bonding; (d) Parylene deposition; (e) Fabricated electrode.

C. Evanescent-mode Cavity

The cavity with the capacitive post is machined from a *Rogers TMM®-3* substrate. The process starts with drilling vias which form the boundary of the resonant cavity and the feeding coplanar waveguide structure. Then a milling-machine is used to create the capacitive post by removing the surrounding substrate material. The vias and the post are then metalized by electroplating 17μm of copper. A second milling removes more substrate material to increase the Q_u of the resonator by reducing dielectric loss. Finally the top copper layer of the cavity and the capacitive post is polished to reduce the surface roughness.

D. Assembly

The SOI diaphragm piece is attached to the cavity by the *118-09A/B-187* conductive silver epoxy from Creative Material, Inc [33]. To accurately control the gap between the post and the diaphragm, the assembly is performed while the resonator is connected to a network analyzer. The resonant frequency is monitored in real time as the diaphragm piece is mounted on the resonator. The position of the diaphragm piece can be adjusted until the desired frequency is achieved. The assembled sample is then cured at room temperate until the solvent content of epoxy precursor fully evaporates. After the

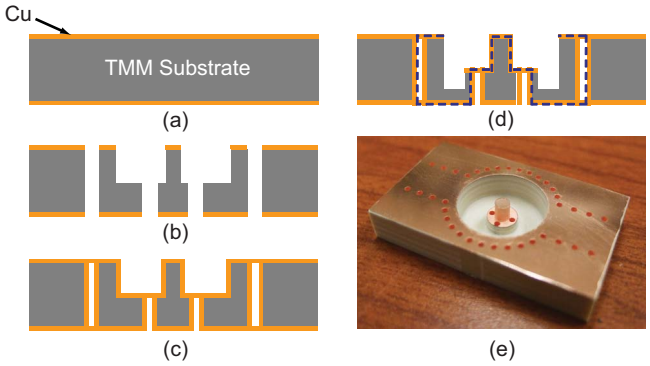

Fig. 13. Fabrication process for evanescent-mode cavity: (a) *TMM®-3* substrate with double side copper laminate; (b) Via and post milling; (c) Cu plating; (d) Cavity milling; (e) Fabricated cavity piece. The dashed line in (d) represent the boundary of the electromagnetic resonant cavity.

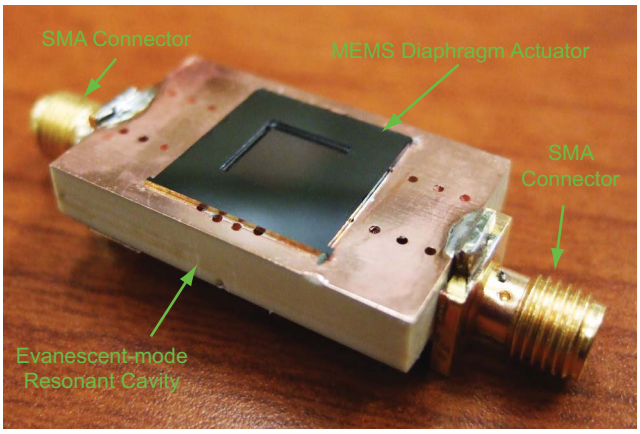

Fig. 14. Fabricated evanescent-mode electromagnetic tunable cavity resonator. The bias electrode in this figure is not permanently fixed to the resonator to reveal the thin diaphragm tuner.

assembly is completed, two SMA connectors are soldered to both ends of the resonator to characterize the RF performance.

From a production stand point, it is desirable to have accurate and repeatable control over the gap. However, the current technology using *TMM®-3* substrate is limited by the surface roughness of the substrate and the copper laminate. A bonding process with a precise vertical alignment is being developed using Si micromachined evanescent-mode cavities. This holds great promise in achieving a low-cost reliable assembly for tunable resonators.

V. Measurements and Discussion

A. Actuation Measurement

The deflection of the thin diaphragm under different bias voltages is measured with an Olympus LEXT® microscope that has a measurement uncertainty of < 0.1 μm. Fig. 15(a) shows the measurement setup. The bias electrode is placed underneath the diaphragm tuner. Bias voltages ranging between $0-130$ V are applied to actuate the diaphragm. The deflection of the center point of the diaphragm is recorded with the LEXT at each bias voltage.

Fig. 15(b) shows the measured deflection-voltage profile. A maximum deflection of 14.3 μm is achieved before pull-in at

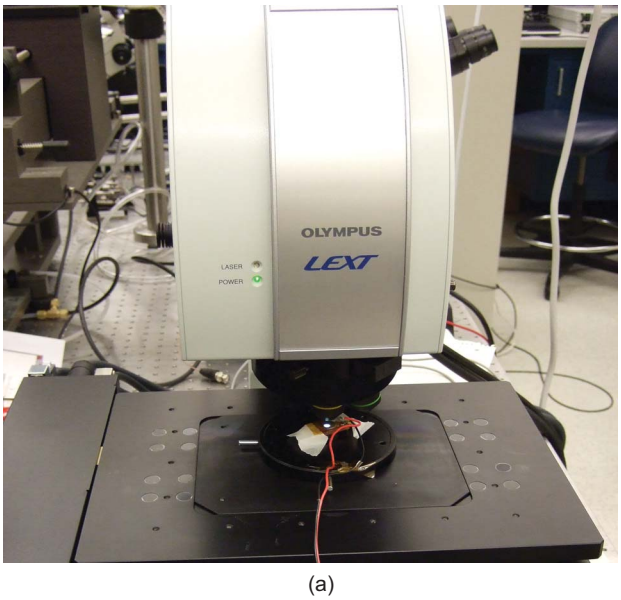

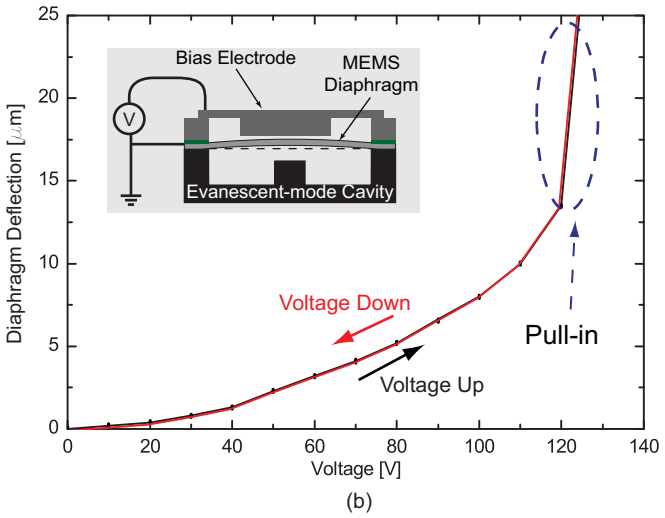

Fig. 15. Deflection-voltage measurement of the MEMS thin diaphragm tuner. A maximum deflection of 14.3 μm is achieved.

122 V. The large range of diaphragm movement ensures a high tuning range for the tunable resonator. The extracted initial gap g_0 and bias gap d_0 are 1.8 ± 0.01 μm and 40 ± 2 μm respectively. No hysteresis is observed in the analog tuning region.

B. RF Measurements

The RF measurements of an assembled tunable resonator are taken with an Agilent 8722ES vector network analyzer. The tuning response of the measured resonator is shown in Fig. 16. The resonator is intentionally designed to be weakly coupled for more accurate extraction of the resonant frequency and Q_u.

With less than 120 V bias voltage, the resonant frequency of the tunable resonator can be tuned between $5.0-1.9$ GHz, achieving a tuning ratio of 2.6:1. Although only a selection of measurements are shown in Fig. 16(a), the frequency tuning is fully analog with < 100 kHz precision. A 1-2 mV precision in

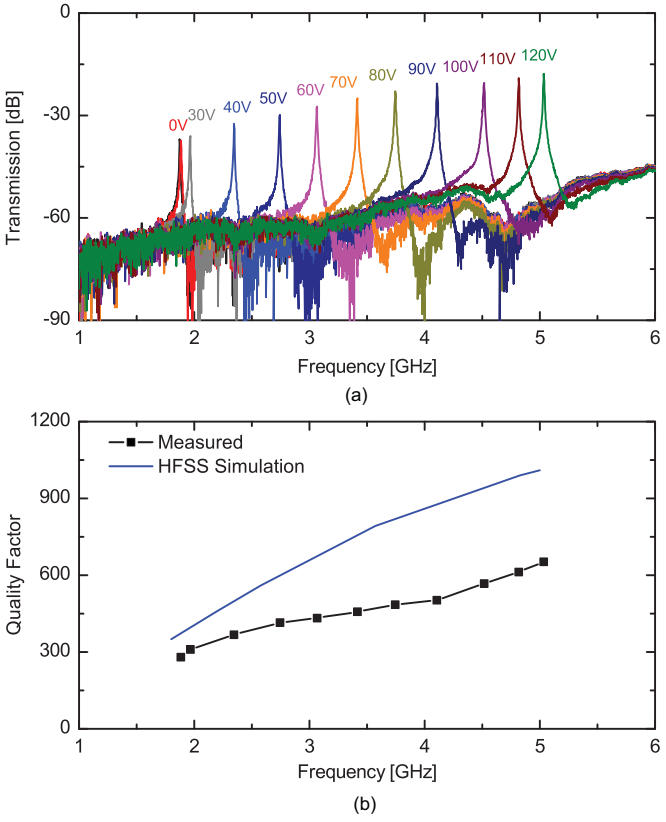

Fig. 16. Measured weakly-coupled transmission (a) and extracted Q_u (b) of the fabricated tunable resonator.

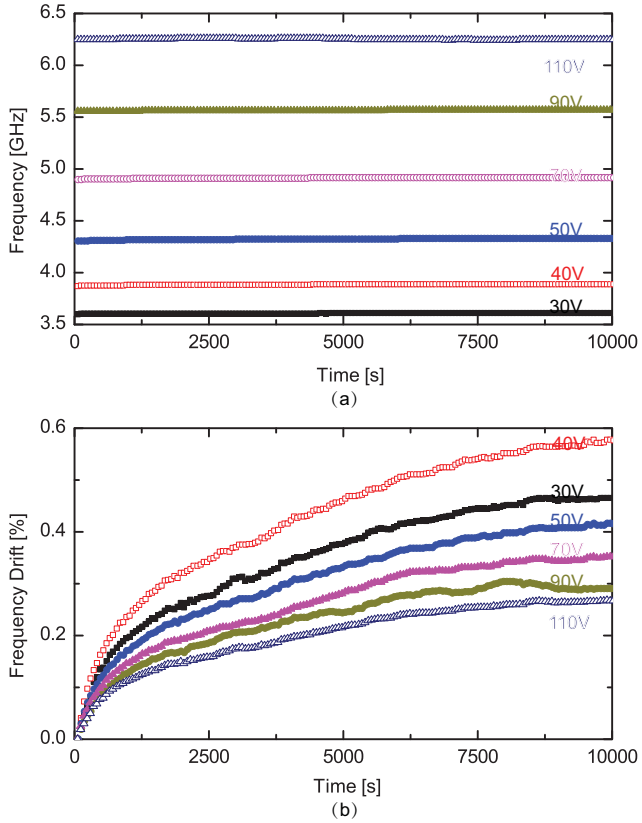

Fig. 17. Measured absolute frequency stability (a) and percentage drift (b) of an evanescent-mode tunable resonator.

the control of bias voltage is required to achieve this frequency precision.

Q_u is extracted using (7).

$$Q_u = \frac{Q_m}{1 - 10^{-IL/10}}, \tag{7}$$

where Q_m is the measured quality factor and IL is the measured insertion loss at the resonant frequency.

With weakly coupled resonators, the extracted Q_u is less sensitive to the measurement accuracy of the insertion loss. The extracted Q_u of the tunable resonators are $300-650$ between $1.9-5.0$ GHz, achieving state-of-the-art performance in MEMS tunable resonators. When compared with simulation, however, the measured Q_u are lower than the simulated ones (Fig. 16(b)) by about 40%. Part of the reason for this reduction is the use of silver epoxy as the intermediate bonding material. The conductivity of the silver epoxy is around 2×10^6 S/m [33], which is about one order of magnitude lower than those of Au (4.1×10^7 S/m) and Cu (5.8×10^7 S/m). Obviously, the Q_u can be improved by using higher conductivity material for bonding. For example, Au-Au thermal-compression bonding has been shown to preserve the Q_u of electromagnetic cavity resonators [23].

C. Stability Measurements

As discussed in Section III, material creep and viscoelasticity causes material property change over time when constant stress is applied. In MEMS structures this is typically seen when a stimulus is applied over longs periods of time. In the case of this tunable resonator design, material creep in the deflected diaphragm causes a frequency drift if the diaphragm is biased under a constant voltage for several hours. It is therefore important to consider this parameter in the filter design so the filter control becomes as simple as possible. The frequency stability of the fabricated resonators is tested by applying a constant bias voltage on the resonator and continuously recording the resonant frequency. Every two minutes ten samples were averaged to result in a recording.

Fig. 17 shows the measured absolute and percentage frequency drifts at different bias voltages. The tunable resonator exhibits very small frequency drift ($< 0.6\%$ in 3 hours). The frequency drift follows an exponential curve that qualitatively agrees with the anelastivity/creep characteristics observed in [32]. For example, with 40 V bias voltage, the percentage frequency drift is 0.2% at the end of 12 minutes and increases to 0.4% at the end of 62 minutes. In 3 hours, the total drift is less than 0.6% and the drfit rate further decreases afterwards.

It is interesting to note that the resonator exhibits smaller percentage frequency drifts at higher bias levels. The principal reason for this lower percentage frequency drift is that g is larger at larger bias voltages. For example, the diaphragm is 5.7 μm and 16.2 μm away from the post at 40 and 110 V bias respectively. Although the deflection drift due to creep/viscoelasticity is larger at 110 V (extracted to be 93 nm at 2 hours compared to 59 nm at 2 hours of 40 V), the incurred percentage frequency drift is smaller at 110 V bias (Fig. 17).

As discussed in Section. III, a feedback control system is required in real-world applications to compensate for frequency

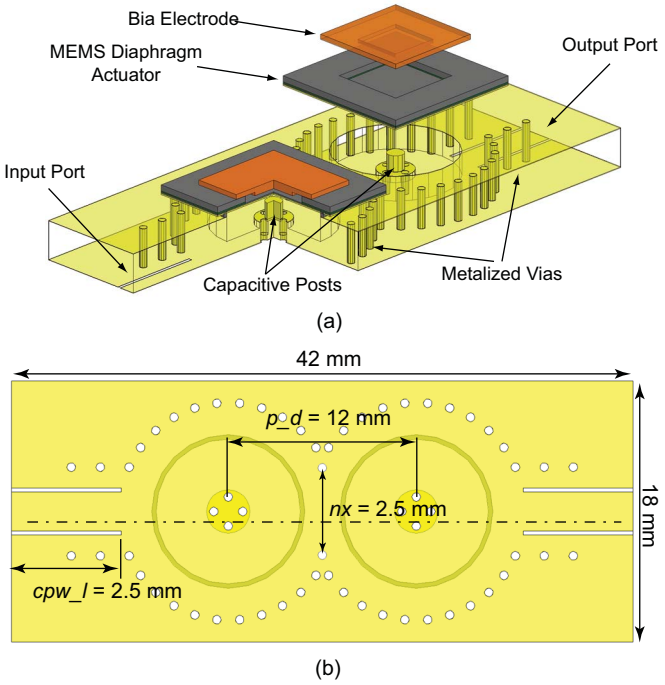

Fig. 18. Design illustration of the 2-pole tunable filter. (a) Bottom view of the designed filter coupling structures; (b) Equivalent circuit of the 2-pole evanescent-mode tunable filter.

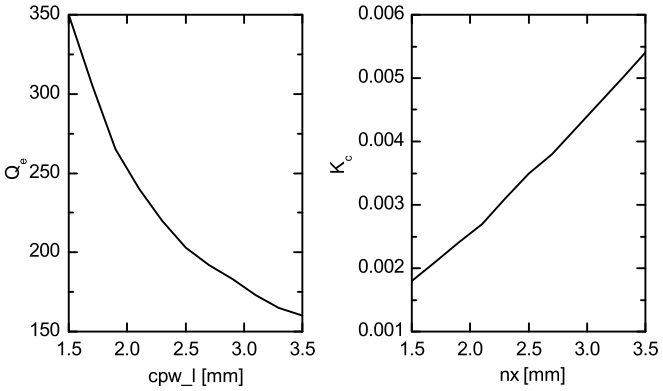

Fig. 19. Simulated relationship between Q_e and cpw_l (a) and k_c and nx (b).

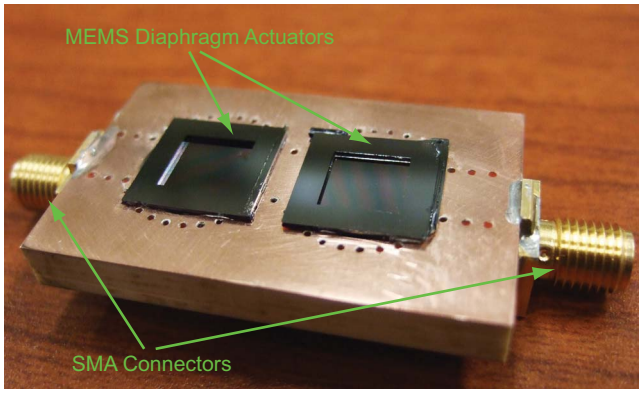

Fig. 20. Fabricated 2-pole evanescent-mode cavity tunable filter.

perturbations due to environmental changes, such as temperature, shock and vibration. The small frequency drift will greatly simplify the design of the feedback control circuitry when the tunable resonator is used in a real-world application.

VI. 2-Pole Evanescent-mode RF MEMS Tunable Filter

A. Design

A 2-pole tunable bandpass Butterworth filter of 0.7 % fractional bandwidth for $3-6$ GHz is designed as a technology demonstrator. Higher order filters can also be designed using the same approach outlined in this section.

Fig. 18(a) shows the concept drawing of the 2-pole filter. Coupling iris formed by metalized vias are used to control coupling strength between the two resonators. As with the resonator design, shorted CPW lines are used as the input and output feed structures.

In designing direct coupled resonator filters, the external quality factor Q_e and the inter-resonator coupling k_c need to be carefully designed to give the desired frequency response. The value of the required Q_e and k_c can be calculated from the Butterworth lowpass prototype [36].

$$Q_e = \frac{g_0 g_1}{\Delta} = 202, \tag{8}$$

$$k_c = \frac{\Delta}{g_1 g_2} = 0.0035, \tag{9}$$

where Δ is the fractional bandwidth and $g_0 = 1$, $g_1 = 1.414$, $g_2 = 1.414$ are the 2nd order Butterworth low-pass prototype values.

Full-wave simulation in HFSS is used to correlate Q_e and k_c with the dimensions of the external and internal coupling structures. Q_e is primarily determined by the length of the shorted CPW feed lines cpw_l. The inter-resonator coupling coefficient k_c is determined by the distance p_d between the two capacitive posts and the opening width of the coupling iris nx. Fig.19 shows the relationship between cpw_l, nx and Q_e, k_c. Critical dimensions of the final design are labeled in Fig. 18(b).

B. Measurements

The filter is fabricated in a similar process as discussed in Section IV. Two separate MEMS diaphragm actuators are packaged on top of two evanescent-mode resonant cavities. Fig. 20 shows the fabricated evanescent-mode tunable filter. Fig. 21 shows the measured tuning response of the fabricated filter.

An Agilent 8722ES network analyzer is used to measure the frequency response of the tunable filter under different bias voltages. Because of assembly tolerances, the g_0 of the two resonators are not identical, leading to different initial resonant frequencies and tuning characteristics. Separate bias voltages are therefore needed to synchronize the resonant frequencies of the two resonators to give the desired bandpass filter response. In tuning the center frequency of the filter, the two bias voltages need to be individually adjusted.

TABLE I
COMPARISON OF TUNABLE FILTER TECHNOLOGIES

	Technology	Center Frequency	Tuning Ratio (%)	Q_u	Impedance	Fabrication Integration	Resistance to Shock/Vibration
This work	MEMS 3D	3.85 GHz	44%	$300-650$	50 Ω	Good	Fair
[18]	MEMS 3D	4.95 GHz	23.7 %	$273-511$	50 Ω	Good	Good
[4]	μ-mechanical	400 kHz	$< 1\%$	$40,000$	$40 - 100$ $k\Omega$	Very good	Very good
[6]	μ-mechanical	810 MHz	2%	$4,000 - 8,000$	59 Ω	Very good	Very good
[8]	MEMS 2.5D	15.5 GHz	3%	$400 - 1600$	50 Ω	Good	Fair
[14]	MEMS Varactor	20 GHz	10%	50	50 Ω	Very good	Good
[11]	BST Varactor	226 MHz	57%	60	50 Ω	Very good	Excellent

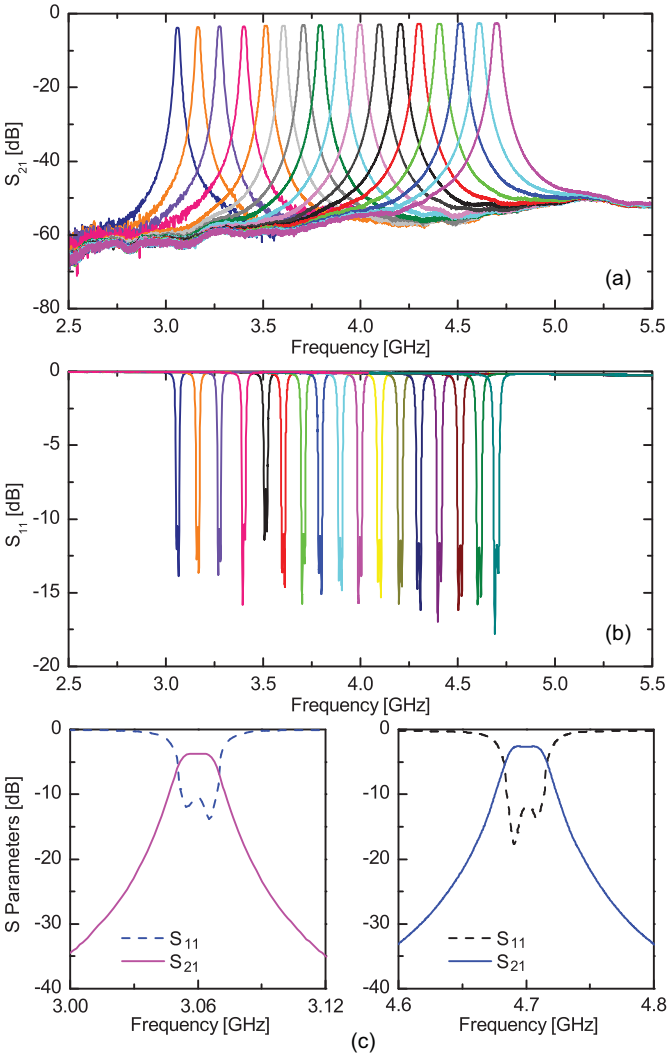

Fig. 21. Measured frequency response ((a) S_{21} and (b) S_{11}) of the evanescent-mode tunable filter under different bias voltages. Close-up views of the passband response at the lower end and higher end of the tuning range are shown in (c).

Although only a selection of data points are shown in Fig. 21, the filter is continuously tunable from $3.04 - 4.71$ GHz, demonstrating a tuning ratio of 1.55:1. Due to fabrication tolerances, the required tuning voltages are less than 140 V, as compared to 120 V in the resonator case. Fig. 22 summarizes

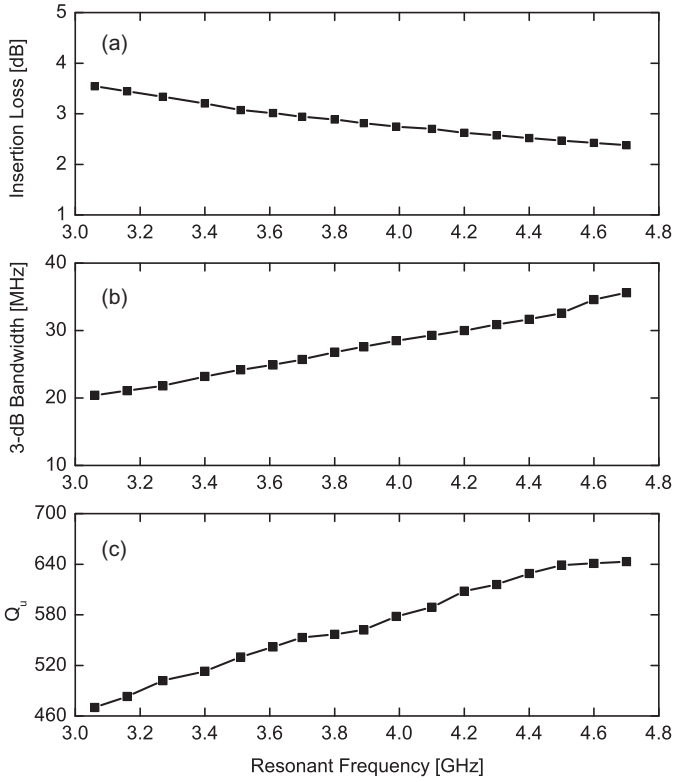

Fig. 22. Measured insertion loss (a), 3-dB bandwidth (b) and the extracted Q_u (c) of the fabricated tunable 2-pole tunable filter.

the performance of the fabricated tunable filter. The tunable filter demonstrates Q_u of $470 - 645$, with insertion loss of $3.55 - 2.38$ dB and 3-dB bandwidth of $20.4 - 35.6$ MHz across the tuning range. These results are compared with other tunable filter technologies in Table. I. Our results represent the state-of-the-art performances in MEMS tunable filters at microwave frequencies.

VII. CONCLUSION

The modeling, design and fabrication techniques for MEMS-enabled widely tunable, high-Q_u evanescent-mode cavity resonators and filters are presented in this paper. Electrostatic actuation of SOI-based thin-film MEMS diaphragm enables highly reliable operation with no hysteresis and ex-

cellent mechanical stability. A continuously tunable resonator from 1.9 to 5.0 GHz (2.6:1 tuning ratio) with Q_u of $300-650$ is demonstrated. The required electrostatic voltage is less than 120 V. A 2-pole continuously tunable filter is also designed and measured covering $3.04-4.71$ GHz (1.55:1 tuning ratio) with insertion loss of $3.55-2.38$ dB for a 3-dB bandwidth of 0.7%. Further advancement of the low-temperature bonding techniques will result in even higher quality factors and reduced RF losses for the resonators and filters. Research on improving the bonding technology is currently underway.

REFERENCES

[1] X. Liu, L. P. B. Katehi, W. J. Chappell, D. Peroulis, "A 3.4-6.2 GHz Continuously Tunable Electrostatic MEMS Resonator with Quality Factor of 460-530", *2009 IEEE MTT-S International Microwave Symposium*, Boston, MA USA, June 2009.

[2] H. Arslan, *Cognitive Radio, Software Defined Radio, and Adaptive Wireless Systems*, Springer, 2007.

[3] W. J. Keane, "YIG filters aid wide open receivers", *Microwave J.*, vol. 17, no. 8, September 1980.

[4] K. Wang, C. T.-C. Nguyen, "High-order medium frequency micromechanical electronic filters", *Journal of Microelectromechanical Systems* , vol.8, no.4, pp.534-556, December 1999

[5] S. Pourkamali, R. Abdolvand, G. K. Ho, F. Ayazi, "Electrostatically coupled micromechanical beam filters", *17th IEEE International Conference on Micro Electro Mechanical Systems (MEMS)*, pp. 584-587, 2004

[6] H. Chandrahalim, D. Weinstein, L. F. Cheow, S. A. Bhave, "High-k dielectrically transduced MEMS thickness shear mode resonators and tunable channel-select RF filters", *Sensors and Actuators A*, vol.136, no.2, pp. 527-539, 2007

[7] W. D. Yan, R. R. Mansour, "Micromachined Millimeter-wave Ridge Waveguide Filter with Embedded MEMS Tuning Elements,", *2006 IEEE MTT-S Int. Microwave Symp. Dig.*, vol., no., pp.1290-1293, 11-16 June 2006

[8] W. D. Yan, R. R. Mansour, "Tunable Dielectric Resonator Bandpass Filter With Embedded MEMS Tuning Elements,", *IEEE Trans. Microwave Theory & Tech.*, vol.55, no.1, pp.154-160, Jan. 2007

[9] A. R. Brown, G. M. Rebeiz, "A varactor-tuned RF filter", *IEEE Trans. Microwave Theory & Tech.*, vol.48, no.7, pp.1157-1160, Jul 2000.

[10] F. A. Miranda, G. Subramanyam, F. W. van Keuls, R. R. Romanofsky, J. D. Warner, C. H. Mueller, "Design and development of ferroelectric tunable microwave components for Ku and K-band satellite communication systems", *IEEE Trans. Microwave Theory & Tech.*, vol.48, no.7, pp.1181-1189, Jul 2000

[11] A. Tombak, J.-P. Maria, F. T. Ayguavives, Z. Jin, G. T. Stauf, A. I. Kingon, A. Mortazawi, "Voltage-controlled RF filters employing thin-film barium-strontium-titanate tunable capacitors", *IEEE Trans. Microwave Theory & Tech.*, vol.51, no.2, pp. 462-467, Feb. 2003

[12] J. Nath, D. Ghosh, J.-P. Maria, A. I. Kingon, W. Fathelbab, P. D. Franzon, M. B. Steer, "An electronically tunable microstrip bandpass filter using thin-film Barium-Strontium-Titanate (BST) varactors", *IEEE Trans. Microwave Theory & Tech.*, vol.53, no.9, pp. 2707-2712, Sept. 2005

[13] D. Peroulis, S. Pacheco, K. Sarabandi, L. P. B. Katehi, "MEMS devices for high isolation switching and tunable filtering", *2000 IEEE MTT-S Int. Microwave Symp. Dig.*, vol.2, no., pp.1217-1220 vol.2, 2000

[14] A. Abbaspour-Tamijani, L. Dussopt, G. M. Rebeiz, "Miniature and tunable filters using MEMS capacitors", *IEEE Trans. Microwave Theory & Tech.*, vol.51, no.7, pp. 1878-1885, July 2003

[15] A. Pothier, J.-C. Orlianges, G. Zheng, C. Champeaux, A. Catherinot, D. Cros, P. Blondy, J. Papapolymerou, "Low-loss 2-bit tunable bandpass filters using MEMS DC contact switches", *IEEE Trans. Microwave Theory & Tech.*, vol.53, no.1, pp. 354-360, Jan. 2005

[16] S. M. Hou, J. H. Lang, A. H. Slocum, A. C. Weber, and J. R. White, " A High-Q Widely Tunable Gigahertz Electromagnetic Cavity Resonator", *J. Microelectromech. Syst.*, vol. 15, no. 6, pp. 1540-1545, December 2006.

[17] H. Joshi, H. H. Sigmarsson, D. Peroulis, and W. J. Chappell, "Highly Loaded Evanescent Cavities for Widely Tunable High-Q Filters", *2007 IEEE MTT-S Int. Microwave Symp. Dig.*, pp. 2133-2136, June 2007.

[18] S.-J. Park, I. Reines, and G. M. Rebeiz, "High-Q RF-MEMS tunable evanescent-mode cavity filter", *2008 IEEE MTT-S International Microwave Symposium*, Boston, MA USA, June 2009.

[19] T.S. Low, W. Guo, "Modeling of a three-layer piezoelectric bimorph beam with hysteresis",*J. Microelectromech. Syst.*, vol.4, no.4, pp.230-237, Dec 1995.

[20] E. Cattana, T. Haccarta, G. Velua, D. Remiensa, C. Bergaudb, L. Nicub ,"Piezoelectric properties of PZT films for microcantilever",*Sensors and Actuators A: Physical*, Vol. 74, Issues 1-3, pp. 60-64, April 1999,

[21] S. Trolier-McKinstry, P. Muralt, "Thin Film Piezoelectrics for MEMS", *Journal of Electroceramics*, Vol. 12, no. 1-2, January 2004.

[22] I. Mayergoyz, G.Bertotti, *The Science of Hysteresis*, Elsevier, 2005

[23] T. A. Schwarz, and L. P. B. Katehi, "A Micromachined Evanescent Mode Resonator", *1999 European Microwave Conference Dig.*, vol. 2, pp. 403-406, October 1999.

[24] X. Gong, A. Margomenos, B. Liu, S. Hajela, L. P. B. Katehi and W. J. Chappell, "Precision Fabrication Techniques and Analysis on Hihg-Q Evanescent-Mode Resonators and Filters of Different Geometries," *IEEE Trans. Microwave Theory & Tech.*, vol. 52, no. 11, pp. 2557-2566, November 2004.

[25] R. G. Carter, J. Feng, U. Becker, "Calculation of the Properties of Reentrant Cylindrical Cavity Resonators", *IEEE Trans. Microwave Theory & Tech.*, vol. 55, no. 12, pp. 2531-2538, December 2007.

[26] High Frequency Structure Simulator, Ansoft Cooperation. http://www.ansoft.com/products/hf/hfss/

[27] G. M. Rebeiz, *RF MEMS, Theory, Design and Technology*, New York: J. Wiley & Sons, 2003.

[28] Rogers Corporation,TMM® Thermoset Microwave Laminates, http://www.rogerscorp.com/acm/products/14/TMM-Thermoset-Microwave-Laminates-Thermoset-ceramic-loaded-plastic.aspx

[29] W. C. Young, R. J. Roark, R. G. Budynas, *Roark's Formulas for Stress and Strain*, 7th Ed., New York: McGraw-Hills, 2002.

[30] S. D. Senturia, *Microsystem Design*, Kluwer Academic Pub., 2000.

[31] F. A. McClintock, A. S. Argon, *Mechanical Behavior of Materials*, TechBooks (reprinted by arrangement with Addison-Wesley Publishing Company, Inc.), Fairfax, VA, 1965, Chapter 12, pp. 432-434 and Chapter 19, pp 640-644.

[32] X. Yan, W.L. Brown, Y. Li, J. Papapolymerou, C. Palego, J. C. M. Hwang, R. P. Vinci, "Anelastic Stress Relaxation in Gold Films and Its Impact on Restoring Forces in MEMS Devices", *J. Microelectromechanical Syst.*, vol.18, no.3, pp.570-576, June 2009

[33] Creative Materials Inc. 118-09A/B-187 Solvent-Resistant Electrically Conductive Ink http://server.creativematerials.com/datasheets/DS_118_09A_B187.pdf

[34] Coventor Inc. http://www.coventor.com

[35] H. H. Sigmarsson, A. Christianson, H. Joshi, S. Moon, D. Peroulis, W. J. Chappell, "In-Situ Control of Tunable Evanescent-Mode Cavity Filters Using Differential Mode Monitoring", *2008 IEEE MTT-S International Microwave Symposium*, Boston, MA USA, June 2009.

[36] G. L. Matthaei, L. Young, E. M. T. Jones, *Microwave Filters, Impedance-Matching Networks and Coupling Structures*, New York: McGraw-Hill, 1964.

Xiaoguang Liu (S'07) received the Bachelor's degree in electrical engineering from Zhejiang University, China in 2004 and is currently working toward the Ph.D. degree at Purdue University, West Lafayette, IN.

His research interests include novel RF MEMS devices and high-Q tunable filters for reconfigurable radio frontends.

He is the recipient of the 2009 Antenna and Propagation Society Graduate Research Fellowship.

Linda P. B. Katehi (S'81-M'84-SM'89-F'95) is currently the Chancellor at the University of California at Davis. She has authored or coauthored over 600 papers published in refereed journals and symposia proceedings, as well as nine book chapters. She holds 13 U.S. patents. Her research is focused on the development and characterization of 3-D integration and packaging of integrated circuits with a particular emphasis on MEMS devices, high-Q evanescent mode filters, and the theoretical and experimental study of planar circuits for hybrid-monolithic and monolithic oscillators, amplifiers, and mixer applications.

Prof. Katehi is a member of the National Academy of Engineering, the Nominations Committee for the National Medal of Technology, the Kauffman National Panel for Entrepreneurship, the National Science Foundation (NSF) Advisory Committee to the Engineering Directorate, and numerous other engineering and scientific committees. She has been the recipient of numerous national and international technical awards and to distinctions as an educator.

William J. Chappell (S'98-M'02) received the B.S.E.E., M.S.E.E., and Ph.D. degrees from The University of Michigan at Ann Arbor, in 1998, 2000, and 2002, respectively.

He is currently an Associate Professor with the Electrical and Computer Engineering Department, Purdue University, West Lafayette, IN, and is also a member of the Birck Nanotechnology Center and the Center for Wireless Systems and Applications. His research focus is on advanced applications of RF and microwave components. He has been involved with numerous Defense Advanced Research Projects Agency (DARPA) projects involved in advanced packaging and materials processing for microwave applications. His research sponsors include Homeland Security Advanced Research Projects Agency (HSARPA), Office of Naval Research (ONR), National Science Foundation (NSF), the State of Indiana, Communications-Electronics Research, Development, and Engineering Center (CERDEC), U.S. Army Research Office (ARO), as well as industry sponsors. His research group uses electromagnetic analysis, unique processing of materials, and advanced design to create novel microwave components. His specific research interests are the application of very high-quality and tunable components utilizing package-scale multilayer components. In addition, he is involved with high-power RF systems, packages, and applications.

Dr. Chappell was the recipient of the URSI Young Scientist Award, the Joel Spira Teaching Excellence Award, and the Eta Kappa Nu 2006 Teacher of the Year Award presented by Purdue University.

Dimitrios Peroulis (S'99-M'04) received the Diploma degree in electrical and computer engineering from the National Technical University of Athens, Athens, Greece, in 1998, and the M.S.E.E. and Ph.D. degrees in electrical engineering from The University of Michigan, Ann Arbor, in 1999 and 2003, respectively.

He is currently an Associate Professor with the School of Electrical and Computer Engineering, Purdue University, West Lafayette, IN. His research work is focused on microelectromechanical systems (MEMS) for multifunctional communications systems and sensors. His group is currently part of two research centers funded by DARPA (IMPACT center) and the National Nuclear Security Administration (PRISM center) that are focused on MEMS failure mechanisms and reliability.